

Research Article

Electronic transitions and energy band structure of $\text{CuGa}_x\text{Al}_{1-x}\text{Se}_2$ crystalsA. Maşnik^a, V. Zalamai^b, V. Ursaki^{b,*}^a Department of Electronics and Telecommunications, Technical University of Moldova, 168, Stefan Cel Mare Av., Chisinau, MD, 2004, Republic of Moldova^b National Center for Materials Study and Testing, Technical University of Moldova, 168, Stefan Cel Mare Av., Chisinau, MD, 2004, Republic of Moldova

ARTICLE INFO

Keywords:

CuGa_xAl_{1-x}Se solid solutions
Optical reflectance spectra
Energy band structure
Brillouin zone
Critical points

ABSTRACT

Optical reflectance spectra have been investigated at photon energies higher than the band gap of $\text{CuGa}_x\text{Al}_{1-x}\text{Se}$ solid solutions with x values varying from 0 to 1. The spectral dependence of the real ϵ_1 and imaginary ϵ_2 dielectric functions was calculated from experimental reflectivity spectra by means of Kramers–Kronig relations. The behavior of features observed in reflectivity spectra and in the spectral dependence of the dielectric functions was analyzed as a function of the solid solution composition. The experimentally observed peaks have been tabulated and related to the electronic band structure of materials computed in previous works.

1. Introduction

The crystal structure of $\text{A}^{\text{I}}\text{B}^{\text{III}}\text{C}^{\text{VI}}_2$ compounds is related to the zinc blende $\text{A}^{\text{II}}\text{B}^{\text{VI}}$ materials, since they can be viewed as an alternative stack of two zinc blende cells with two cations A^{I} and B^{III} instead of the A^{II} cation, which results in a non-centrosymmetric D_{2d}^7 space group structure with anisotropy of optical properties. The anisotropy of these materials and their inherent birefringence makes them suitable for the development of optical filters [1–10]. Apart from that, narrow bandgap materials like $\text{CuIn}_{1-x}\text{Ga}_x\text{Se}_2$ are used in solar cells [11–14], while prospects for nonlinear optics applications have been demonstrated for wider bandgap compounds, such as AgGaS_2 and AgGaSe_2 [15–23]. Nanostructured $\text{A}^{\text{I}}\text{B}^{\text{III}}\text{C}^{\text{VI}}_2$ compounds are also used in light-emitting devices [24,25] and photocatalysis [26,27].

The availability of data concerning the energy band structure of these materials is a key point for a series of applications including the development of microelectronic and optoelectronic devices. Among other experimental tools, optical spectroscopy is a versatile, non-destructive and simple method to provide such information. Exciton parameters at the center of the Brillouin zone have been studied by optical reflectance spectroscopy in a series of $\text{CuIn}_{1-x}\text{Ga}_x\text{S}_2$, $\text{CuIn}_{1-x}\text{Ga}_x\text{Se}_2$, and $\text{CuAl}_{1-x}\text{Ga}_x\text{Se}_2$ quaternary solid solutions [28,29], in addition to highly focused investigation of this issue in ternary end-point compounds with $x = 0$ and $x = 1$. As concerns electronic transitions at other critical point of the Brillouin zone, they have been investigated at the T and N critical-points in $\text{CuIn}_{1-x}\text{Ga}_x\text{S}_2$, $\text{CuIn}_{1-x}\text{Ga}_x\text{Se}_2$, and $\text{CuIn}_{1-x}\text{Al}_x\text{Se}_2$ solid solutions [28,30]. In ternary end-point compounds, electronic structure and inter-band transitions have been investigated at the T and N

critical-points in CuInS_2 , CuGaS_2 , CuInSe_2 , CuGaSe_2 , and CuAlSe_2 [31, 32], as well as at Z, X, P, N critical-points in CuInS_2 , CuGaS_2 , CuGaSe_2 , CuAlS_2 , and CuAlSe_2 crystals [33–36].

The experimentally observed electronic transitions in spectroscopic ellipsometry or optical reflectance spectroscopy have been interpreted on the basis of theoretical calculations of the electronic structure. The electronic structure of ternary $\text{A}^{\text{I}}\text{B}^{\text{III}}\text{C}^{\text{VI}}_2$ chalcopyrite semiconductors with $\text{A} = \text{Cu}$; $\text{B} = \text{In, Ga, Al}$; and $\text{C} = \text{S, Se}$ at the T, Γ , and N points of the Brillouin zone has been calculated self consistently within the density-functional formalism with a potential-variation mixed-basis (PVMB) approach around 40 years ago [37]. Later-on, electronic structure of some compounds has been computed at other points of the Brillouin zone using the method of full-potential linear muffin-tin orbital (FPLMTO) in Ref. [38], and the linear combination of atomic orbitals scheme within density functional theory (LCAO–DFT) and full-potential linearized augmented plane wave (FP-LAPW) methods in Refs. [39,40]. Particularly, the features observed in experimentally measured optical reflectance spectra and those of dielectric functions deduced from these spectra by means of Kramers–Kronig relations in CuGaS_2 , CuInS_2 , and CuGaSe_2 [33,34] as well as in CuAlS_2 and CuAlSe_2 [35,36] were previously interpreted on the basis of a generic band diagram for $\text{A}^{\text{I}}\text{B}^{\text{III}}\text{C}^{\text{VI}}_2$ compounds deduced from electronic structure calculated by the FPLMTO method [38]. However, the univocal assignment of features observed in experimental spectra to electronic transitions at critical-points of the band structure was complicated because of very close values of some energy intervals between the valence and conduction bands.

The goal of this paper is to make use of a comparison of trends in the

* Corresponding author.

E-mail address: vvursaki@gmail.com (V. Ursaki).

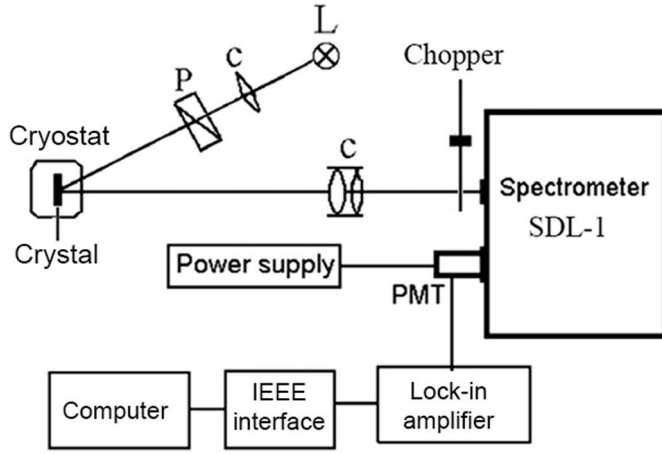


Fig. 1. Experimental set-up scheme for measurements of optical reflectance spectra.

energy band structures of $\text{CuAl}_{1-x}\text{Ga}_x\text{Se}_2$ solid solutions as a function of the x -value for a more reliable assignment of experimentally observed electronic transitions to specific critical points of the previously proposed generic band structure diagram.

2. Sample preparation, experimental details, and methodology of dielectric functions calculation

$\text{CuAl}_{1-x}\text{Ga}_x\text{Se}_2$ crystals with mirror-like surfaces containing the optical c -axis have been grown by chemical vapor transport [29]. They were mounted on the cold stage of a cryostat, and the reflectance spectra were measured with an installation which scheme is illustrated in Fig. 1. A halogen or a hydrogen lamp served as light sources (L). The light from the lamp was polarized by a Glan–Thomson polarization prism (P) and focused by a condenser (C) to the sample surface. The reflected light from the sample surface was modulated by a chopper and focused by another condenser at the entrance slit of SDL-1 spectrometer. The signal from a photomultiplier tube was registered by a lock-in amplifier and transmitted via an IEEE interface to a computer for data processing.

The anisotropy of optical properties of $\text{CuAl}_{1-x}\text{Ga}_x\text{Se}_2$ crystals was revealed from the investigation of spectral dependences of dielectric functions in $E||c$ and $E\perp c$ polarizations. The spectral dependences of the real ϵ_1 and imaginary ϵ_2 dielectric functions were calculated from experimental reflectivity spectra by means of Kramers–Kronig relations taking into account that

$$r = \frac{n - ik - 1}{n - ik + 1} = \sqrt{Re^{-i\phi}} \quad (1)$$

where r is the complex reflectivity, R is the measured reflectivity, n is the real refractive index, k is the extinction coefficient, and ϕ is the phase angle.

The phase angle is calculated as:

$$\phi(\omega_0) = \frac{\omega_0}{\pi} \int_0^{\infty} \frac{\ln R(\omega)}{\omega_0^2 - \omega^2} d\omega. \quad (2)$$

Experimentally, the reflectivity R was measured in a limited spectral range $a \leq \omega \leq b$. In our case measurements have been performed in a spectral range from 2.0 eV to 6.5 eV. In the high-energy region an approximation of the spectral dependence of the reflection coefficient is used to calculate the dielectric constants using an analytic function. A simple approximation was used: $R(\omega) = R(a)$ for $0 \leq \omega \leq a$ and $R(\omega) = c\omega^{-p}$ for $b \leq \omega \leq \infty$, where c and p are constants according to Ref. [34].

Knowing the experimental spectrum $R(\omega)$ and the function $\phi(\omega)$ calculated according to eq. (2), the optical constants were calculated as

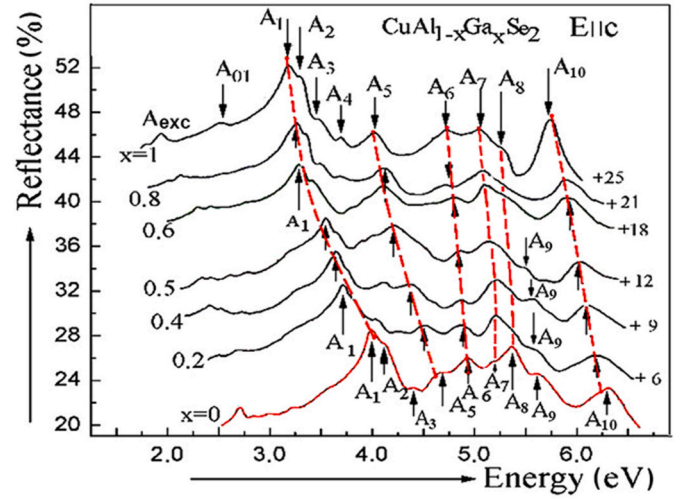


Fig. 2. Optical reflectance spectra measured in $E||c$ polarization for $\text{CuGa}_x\text{Al}_{1-x}\text{Se}$ crystals at temperature of 77 K.

$$\epsilon_1 = n^2 - k^2, \text{ and } \epsilon_2 = 2nk, \quad (3)$$

where

$$n = \frac{1 - R}{1 - 2\sqrt{R}\cos\phi + R}, k = \frac{2\sqrt{R}\sin\phi}{1 - 2\sqrt{R}\cos\phi + R}. \quad (4)$$

3. Experimental results and discussions

Fig. 2 shows spectral dependences of reflectance spectra measured in $E||c$ polarization for $\text{CuGa}_x\text{Al}_{1-x}\text{Se}$ crystals with various compositions from $x = 0$ (CuAlSe_2) to $x = 1$ (CuGaSe_2).

The observed peaks in the reflectance spectra are related to electron transitions at specific points of the valence and conduction bands. Therefore, data related to the energy band structure of $\text{CuGa}_x\text{Al}_{1-x}\text{Se}$ solid solutions can be extracted from the spectral position of features observed in the reflectance spectra, which are connected to features of the complex dielectric function.

The imaginary part of the complex dielectric function is determined by the optical transition probability W_{CV} according to the expression below [9,10]:

$$\epsilon_2(\omega) = \frac{2\hbar}{E_0^2 \epsilon_0} W_{CV}. \quad (5)$$

where E_0 is the amplitude of the electric field.

The optical transition probability W_{CV} is given by the following expression:

$$W_{CV} = \frac{4\pi}{\hbar} \frac{e^2}{m_c^2} \frac{A_0^2}{(2\pi)^3} \int |\Pi_{CV}^e|^2 \delta(E_C - E_V - \hbar\omega) d^3k, \quad (6)$$

where A_0 is the amplitude of the vector potential, which is related to the electric field as:

$$\vec{E} = -\frac{\partial \vec{A}}{\partial t} = A_0 \vec{e} \omega \sin(\vec{k} \cdot \vec{r} - \omega t), \quad (7)$$

It follows from eqs (5) and (7) that:

$$\epsilon_2(\omega) = \frac{e^2}{m_c^2 \omega^2 \pi^2 \epsilon_0} \int |\Pi_{CV}^e|^2 \delta(E_{CV} - \hbar\omega) d^3k, \quad (8)$$

where δ -function implies the fulfillment of energy conservation law. The first necessary condition for electron transitions to occur between the valence and conduction bands is the requirement that the photon energy

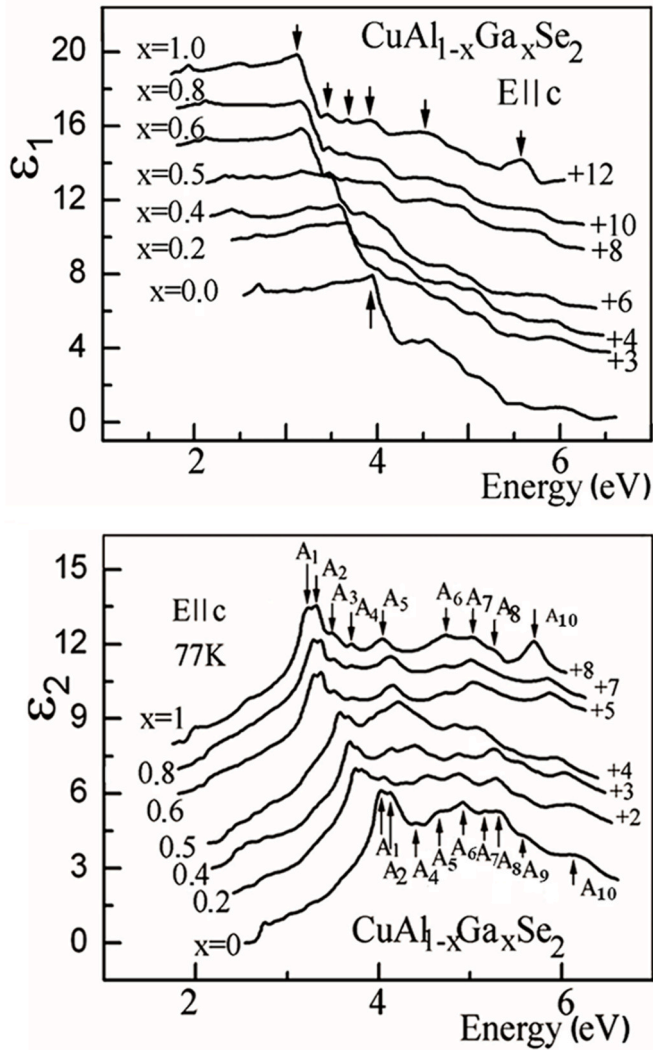


Fig. 3. Spectral dependences of optical functions ϵ_1 and ϵ_2 in E||c polarization for $\text{CuGa}_x\text{Al}_{1-x}\text{Se}$ crystals calculated from experimentally measured spectra in Fig. 2 according to Kramers–Kronig relations.

is in resonance with energetic intervals E_C-E_V . Apart from that, the matrix element $\Pi_{CV}^e \neq 0$ should be different from zero, and according to the momentum conservation law for direct transitions, it should be $\Delta k = k_V - k_C = 0$. The imaginary component of the complex dielectric function $\epsilon_2(\omega)$ depends on the magnitude of the matrix element $|\Pi_{CV}^e|^2$, which is

Table 1

Energies of electronic transitions in $\text{CuGa}_x\text{Al}_{1-x}\text{Se}$ crystals determined both from reflectance spectra and from features in the dielectric function ϵ_2 in the E||c polarization.

X value		A ₁	A ₂	A ₃	A ₄	A ₅	A ₆	A ₇	A ₈	A ₉	A ₁₀
0.0	R	4.01	4.12		4.40	4.68	4.94	5.21	5.36	5.63	6.31
	ϵ_2	4.02	4.13		4.42	4.65	4.90	5.19	5.35	5.63	6.21
0.2	R	3.71	3.83	4.06	4.27	4.51	4.86	5.20	5.36	5.60	6.19
	ϵ_2	3.75	3.83		4.30	4.51	4.86		5.30	5.58	6.11
0.4	R	3.65	3.75		4.10	4.38	4.87	5.18	5.36	5.56	6.11
	ϵ_2	3.67	3.77		4.17	4.40	4.87		5.27	5.56	5.95
0.5	R	3.56	3.67	3.88	4.01	4.21	4.84	5.14		5.51	6.01
	ϵ_2	3.58	3.69		4.01	4.22	4.82	5.12		5.51	5.99
0.6	R	3.28	3.42	3.59	3.81	4.10	4.80	5.11	5.32		5.93
	ϵ_2	3.31	3.38	3.54	3.75	4.14	4.73	5.09			5.86
0.8	R	3.26	3.35	3.51	3.70	4.12	4.74	5.07			5.88
	ϵ_2	3.29	3.37	3.54	3.73	4.11	4.70	5.05			5.85
1.0	R	3.19	3.29	3.48	3.69	4.02	4.71	5.03	5.27		5.75
	ϵ_2	3.21	3.32	3.50	3.71	4.03	4.71	5.01	5.27		5.70

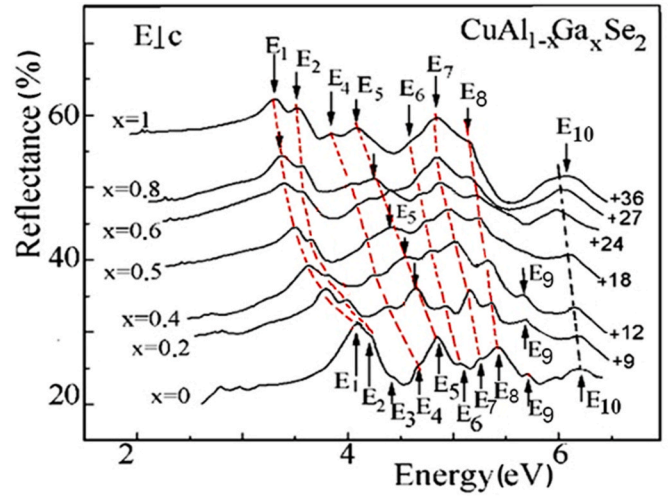


Fig. 4. Optical reflectance spectra measured in E⊥c polarization for $\text{CuGa}_x\text{Al}_{1-x}\text{Se}$ crystals at temperature of 77 K.

determined by the wave functions of the initial and final states participating in the transition. These relations should be analyzed separately for each polarization in anisotropic crystals. Respectively, the value of the imaginary component of the complex dielectric function and the absorption coefficient are considerably higher in the allowed polarization than the respective values in the forbidden polarization.

The feature A_{exc} in the reflectance spectra is caused by the excitonic transitions in the center of the Brillouin zone (Γ point), but the analysis of these transitions is not the topic of this paper, since they have been discussed in a previous paper [29]. The peak A_{01} may come from some indirect transitions, taking into account its weak feature in the reflectance spectrum.

The spectral dependences of the real ϵ_1 and imaginary ϵ_2 components of the complex dielectric function ϵ calculated from the reflectivity spectra using equation (3) for $\text{CuGa}_x\text{Al}_{1-x}\text{Se}$ crystals with various compositions are shown in Fig. 3.

The energetic positions of features $A_1 - A_{10}$ determined from the reflectance spectra in Fig. 2 and from the spectral dependence of the dielectric function ϵ_2 in Fig. 3 are summarized in Table 1.

Fig. 4 shows spectral dependences of reflectance spectra measured in E⊥c polarization for $\text{CuGa}_x\text{Al}_{1-x}\text{Se}$ crystals with various compositions. The comparison of the behavior of peaks in reflectance spectra measured in different polarizations is expected to provide information about the optical anisotropy of $\text{CuGa}_x\text{Al}_{1-x}\text{Se}$ crystals. Features similar to those of Fig. 2 are observed in Fig. 4, but at slightly different spectral positions.

The spectral dependences of the real ϵ_1 and imaginary ϵ_2 components

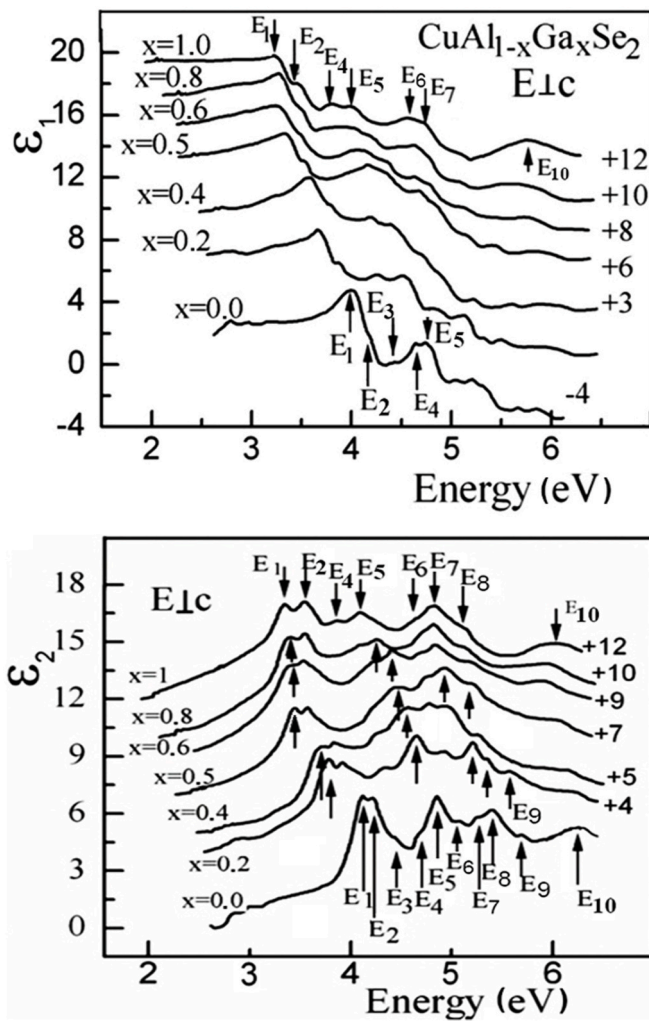


Fig. 5. Spectral dependences of optical functions ϵ_1 and ϵ_2 in $E_{\perp c}$ polarization for $\text{CuGa}_x\text{Al}_{1-x}\text{Se}$ crystals calculated from experimentally measured spectra in Fig. 4 according to Kramers–Kronig relations.

of the complex dielectric function in the $E_{\perp c}$ polarization were calculated from the reflectivity spectra of Fig. 4, and they are presented in Fig. 5.

The energetic positions of features $E_1 - E_{10}$ determined from the reflectance spectra in Fig. 4 and from the spectral dependence of the dielectric function ϵ_2 in Fig. 5 are summarized in Table 2.

The peaks A_1, A_2 , as well as E_1, E_2 are related to electron transitions

Table 2

Energies of electronic transitions in $\text{CuGa}_x\text{Al}_{1-x}\text{Se}$ crystals determined both from reflectance spectra and from features in the dielectric function ϵ_2 in the $E_{\perp c}$ polarization.

X value		E_1	E_2	E_3	E_4	E_5	E_6	E_7	E_8	E_9	E_{10}
0.0	R	4.10	4.24	4.42	4.68	4.86	5.02	5.19	5.45	5.72	6.26
	ϵ_2	4.12	4.23	4.45	4.69	4.85	5.06	5.25	5.40	5.71	6.29
0.2	R	3.73	3.90		4.46	4.65	4.90	5.13	5.40	5.68	6.24
	ϵ_2	3.78	3.92		4.33	4.66	4.95	5.18	5.37	5.64	6.25
0.4	R	3.63	3.81		4.29	4.54	4.80	5.03	5.37	5.65	6.19
	ϵ_2	3.72	3.83		4.28	4.56	4.76	5.00	5.36		6.12
0.5	R	3.40	3.55		4.19	4.43	4.75	4.97	5.24		6.13
	ϵ_2	3.45	3.59		4.25	4.45	4.74	4.94	5.22		6.09
0.6	R	3.35	3.54		4.17	4.40	4.70	4.86	5.19		6.02
	ϵ_2	3.40	3.55		4.24	4.42	4.73	4.85	5.16		5.92
0.8	R	3.33	3.56		4.00	4.25	4.65	4.85	5.13		6.03
	ϵ_2	3.40	3.54		4.01	4.26	4.70	4.84	5.12		5.99
1.0	R	3.30	3.51		3.85	4.10	4.60	4.83	5.13		5.99
	ϵ_2	3.33	3.54		3.84	4.11	4.65	4.84	5.11		5.96

in the center of the Brillouin zone from the V_1 and V_3 valence bands to the C_2 conduction band, respectively, since these are the narrowest interband intervals in the band structure illustrated in Fig. 6, except for the electronic transitions to the C_1 conduction band, related to excitonic transitions, marked as A_{exc} in Fig. 2.

The next intervals correspond to the Z and P critical-points, and the energies of these intervals are very close to each other. These intervals are slightly larger as compared to those at the Γ -point, but slightly narrower than those situated at the P-point. Taking into account the close values of energy intervals, one can assign the A_3, E_3 peaks to either $Z(V_1) - Z(C_1)$, or $P(V_1) - P(C_1)$ transitions. Similarly, the energy of the electron transition $P(V_2) - P(C_1)$ is very close to that of the $X(V_1) - X(C_1)$ transition. Therefore, the A_4, E_4 peaks can be attributed to either one or another of these transitions. A similar difficulty for unequivocally assignment was mentioned in a previous paper related to electronic transitions in CuGaSe_2 crystals [34]. Apart from that, it was assumed that the peaks A_5, E_5 are caused by transitions from V_1 to C_1 bands at the X point, while the peaks A_6, E_6 are caused by transitions from V_2 to C_1 bands at the same point. However, the analysis of the behavior of the peaks A_5, E_5 and A_6, E_6 in Fig. 2 depending on the composition change of the solid solution from CuGaSe_2 ($x = 1$) to CuAlSe_2 ($X = 0$) suggests that these peaks are related to electronic transitions at different critical-points.

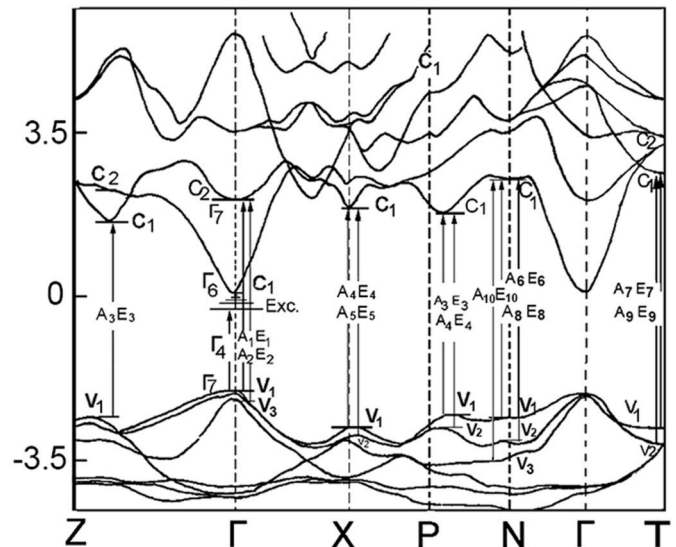


Fig. 6. Assignment and notations for electronic transitions in $\text{CuGa}_x\text{Al}_{1-x}\text{Se}$ crystals according to the band structure of materials computed in previous works.

Table 3
Peaks assignment to electronic transitions.

Peak notation	Electronic transition assignment
A ₁ , E ₁	$\Gamma(V_1) - \Gamma(C_2)$
A ₂ , E ₂	$\Gamma(V_3) - \Gamma(C_2)$
A ₃ , E ₃	$Z(V_1) - Z(C_1)$ or $P(V_1) - P(C_1)$
A ₄ , E ₄	$P(V_2) - P(C_1)$ or $X(V_1) - X(C_1)$
A ₅ , E ₅	$X(V_2) - X(C_1)$
A ₆ , E ₆	$N(V_1) - N(C_1)$
A ₇ , E ₇	$T(V_1) - T(C_1)$
A ₈ , E ₈	$N(V_2) - N(C_1)$
A ₉ , E ₉	$T(V_2) - T(C_1)$
A ₁₀ , E ₁₀	$N(V_3) - N(C_1)$

The shift of the A₅, E₅ peaks position in Figs. 2 and 4 with increasing the x value is much larger as compared to the shift of A₆, E₆ peaks. This is an indicative of their origin from electronic transitions at different critical points, since the increasing band-gap rate with increasing x value is different at different points of the Brillouin zone. One can see that the shift rate for peaks A₁ – A₅ and E₁ – E₅ is generally much larger as compared to that of peaks A₆ – A₁₀ and E₆ – E₁₀. Therefore, we suppose that the peaks A₅, E₅ are related to electronic transitions at the X-point, while the peaks A₆, E₆ come from electronic transitions at the N point. The energy intervals increase in the following sequence $[X(V_2) - X(C_1)] < [N(V_1) - N(C_1)] < [T(V_1) - T(C_1)] < [N(V_2) - N(C_1)] < [T(V_2) - T(C_1)] < [N(V_3) - N(C_1)]$, and the peaks A₅, E₅ to A₁₀, E₁₀ are assigned to these electronic transitions according their spectral positions. The assignment of the observed peaks to electronic transitions is summarized in Table 3.

The anisotropy of optical properties of CuGa_xAl_{1-x}Se solid solutions is indicated by a different behavior of A peaks as compared to E peaks with changing the chemical composition. For instance, the shift of the E₆ – E₈ peaks with increasing x-value is larger than the shift of the A₆ – A₈ peaks, while the shift of the E₁₀ peak is significantly smaller than the shift of the A₁₀ peak.

4. Conclusions

The results of this study demonstrate that the analysis of the behavior of features in optical reflectance spectra of CuGa_xAl_{1-x}Se solid solutions, at photon energies greater than the band gap, as a function of the solid solution composition, facilitates assigning the observed peaks in reflectivity spectra and in spectral dependence of the dielectric functions to specific electronic transitions at various critical points of the Brillouin zone. The peaks at lower photon energies, which were attributed to electronic transitions at the Γ , Z, X, and P points exhibit a trend with a higher rate of shifting with increasing x-value as compared to peaks attributed to electronic transitions at the N and T points. The analysis of the trend for peaks measured in the E_{||}c and E_⊥c polarizations gives information about the anisotropy of optical properties.

CRedit authorship contribution statement

A. Maşnik: Investigation. **V. Zalmai:** Data curation, calculation of dielectric functions from experimental reflectivity spectra, writing original draft, Writing – original draft. **V. Ursaki:** Conceptualization, Methodology, Writing – review & editing.

Declaration of competing interest

The authors declare that they have no known competing financial interests or personal relationships that could have appeared to influence the work reported in this paper.

Acknowledgements

This work was supported financially by the National Agency for Research and Development of the Republic of Moldova under the grant no. 20.80009.5007.20, and by the Horizon-2020 research and innovation programme of the European Union (Grant No. 810652, Nano-MedTwin project).

References

- [1] P. Yeh, Zero crossing birefringent filters, *Opt Commun.* 35 (1980) 15–19, [https://doi.org/10.1016/0030-4018\(80\)90351-X](https://doi.org/10.1016/0030-4018(80)90351-X).
- [2] J.F. Lotspeich, R.R. Stephens, D.M. Henderson, Electrooptic tunable filters for infrared wavelengths, *IEEE J. Quantum Electron.* QE 18 (1982) 1253–1258, <https://doi.org/10.1109/JQE.1982.1071700>.
- [3] H. Horinaka, H. Sonomura, T. Miyauchi, Optical band-pass filter using accidental isotropy and optical activity of AgGaSe₂, *Jpn. J. Appl. Phys.* 24 (1985) 463–466, <https://doi.org/10.1143/JJAP.24.463>.
- [4] T. Yamamoto, H. Takehara, H. Horinaka, T. Miyauchi, Optical band-pass filter using accidental isotropy and optical activity of AgGaSe₂ (II), *Jpn. J. Appl. Phys.* 25 (1986) 1397–1399, <https://doi.org/10.1143/JJAP.25.1397>.
- [5] H. Horinaka, N. Yamamoto, Optical band-elimination filter made of optically active uniaxial crystal of AgGaSe₂ for AlGaAs semiconductor laser, *Proc. SPIE* 1319 (1990), <https://doi.org/10.1117/12.34869>.
- [6] H. Horinaka, N. Yamamoto, H. Hamaguchi, New approach to highly efficient Raman spectroscopy using a laser diode and AgGaSe₂ crystal filter, *Appl. Spectrosc.* 46 (1992) 379–381, <https://www.osapublishing.org/as/abstract.cfm?URI=as-46-2-379>.
- [7] N. Yamamoto, H. Horinaka, Y. Cho, H. Hamaguchi, Application of AgGaSe₂ filter to easy Raman spectroscopy, *Anal. Sci.* 7 (1991) 581–584, J-GLOBAL ID : 201902017357516853 Reference number:19S2778397.
- [8] M. Susaki, N. Yamamoto, H. Horinaka, W.Z. Huang, Y. Cho, Performance of AgGaSe₂ crystal filter for Raman spectroscopy, *Jpn. J. Appl. Phys.* 33 (1994) 1561–1564, <https://doi.org/10.1143/JJAP.33.1561>.
- [9] N. Syrbu, A. Dorogan, V. Ursaki, I. Stamov, I. Tiginyanu, Birefringence of CuGa₂ crystals, *Opt Commun.* 284 (2011) 3552–3557, <https://doi.org/10.1016/j.optcom.2011.03.053>.
- [10] N.N. Syrbu, A.V. Dorogan, A. Masnik, V.V. Ursaki, Birefringence of CuGa_xAl_{1-x}Se₂ crystals, *J. Opt.* 13 (2011), 035703, <https://doi.org/10.1088/2040-8978/13/3/035703>.
- [11] M.A. Green, K. Emery, D.L. King, S. Igari, W. Warta, Solar cell efficiency tables (version 20), *Prog. Photovoltaics Res. Appl.* 10 (2002) 355–360, <https://doi.org/10.1002/pip.453>.
- [12] M.G. Panthani, V. Akhavan, B. Goodfellow, J.P. Schmidtke, L. Dunn, A. Dodabalapur, P.F. Barbara, B.A. Korgel, Synthesis of CuInS₂, CuInSe₂, and Cu(InxGa1-x)Se₂ (CIGS) nanocrystal ‘inks’ for printable photovoltaics, *J. Am. Chem. Soc.* 130 (49) (2008) 16770–16777, <https://doi.org/10.1021/ja805845q>.
- [13] I. Repins, M.A. Contreras, B. Egaas, C. DeHart, J. Scharf, C.L. Perkins, B. To, R. Noufi, 19.9%-efficient ZnO/CdS/CuInGaSe₂ solar cell with 81.2% fill factor, *Prog. Photovoltaics Res. Appl.* 16 (2008) 235–239, <https://doi.org/10.1002/pip.822>.
- [14] P. Jackson, D. Hariskos, E. Lotter, S. Paetel, R. Wuerz, R. Menner, W. Wischmann, M. Powalla, New world record efficiency for Cu(In,Ga)Se₂ thin-film solar cells beyond 20%, *Prog. Photovoltaics Res. Appl.* 19 (2011) 894–897, <https://doi.org/10.1002/pip.1078>.
- [15] D.S. Chempla, P.J. Kupecek, D.S. Robertson, R.C. Smith, Silver thiogallate, a new material with potential for infrared devices, *Opt Commun.* 3 (1971) 29–31, [https://doi.org/10.1016/0030-4018\(71\)90207-0](https://doi.org/10.1016/0030-4018(71)90207-0).
- [16] J.L. Shay, J.H. Wernick, Ternary Chalcopyrite Semiconductors, Pergamon, New York, 1975.
- [17] Y.X. Fan, R.C. Eckardt, R.L. Byer, R.K. Route, R.S. Feigelson, AgGaSe₂ infrared parametric oscillator, *Appl. Phys. Lett.* 45 (1984) 313–315, <https://doi.org/10.1063/1.95275>.
- [18] D.A. Roberts, Dispersion equations for nonlinear optical crystals: KDP, AgGaSe₂, and AgGaSe₂, *Appl. Opt.* 35 (1996) 4677–4688, <https://doi.org/10.1364/AO.35.004677>.
- [19] G.C. Catella, D. Burlage, Crystal growth and optical properties of AgGaSe₂ and AgGaSe₂, *MRS Bull.* 23 (1998) 28–36, <https://doi.org/10.1557/S0883769400029055>.
- [20] P.G. Schunemann, K.L. Schepler, P.A. Budni, Nonlinear frequency conversion performance of AgGaSe₂, ZnGeP₂, and CdGeAs₂, *MRS Bull.* 23 (1998) 45–49, <https://doi.org/10.1557/S0883769400029092>.
- [21] Q.-T. Xu, Z.-D. Sun, Y. Chi, H.-G. Xue, S.-P. Guo, Monoclinic gallium selenide: an AgGaSe₂-type structure variant with balanced infrared nonlinear optical performance, *J. Mater. Chem. C* 7 (2019) 11752–11756, <https://doi.org/10.1039/C9TC03909K>.
- [22] X. Luo, Z. Li, Y. Guo, J. Yao, Y. Wu, Recent progress on new infrared nonlinear optical materials with application prospect, *J. Solid State Chem.* 270 (2019) 674–687, <https://doi.org/10.1016/j.jssc.2018.12.036>.
- [23] J. Wu, W. Huang, H.-G. Liu, Z. He, B. Chen, S. Zhu, B. Zhao, Y. Lei, Xi. Zho, Investigation of the thermal properties and crystal growth of the nonlinear optical crystals AgGaSe₂ and AgGaGeS₄, *Cryst. Growth Des.* 20 (2020) 3140–3153, <https://doi.org/10.1021/acs.cgd.0c00018>.

- [24] B. Chen, N. Pradhan, H. Zhong, From large-scale synthesis to lighting device applications of ternary I–III–VI semiconductor nanocrystals: inspiring greener material emitters, *J. Phys. Chem. Lett.* 9 (2018) 435–445, <https://doi.org/10.1021/acs.jpcclett.7b03037>.
- [25] J.H. Kim, H. Yang, High-Efficiency Cu–In–S quantum-DotLight-emitting device exceeding 7%, *Chem. Mater.* 28 (2016) 6329–6335, <https://doi.org/10.1021/acs.chemmater.6b02669>, 2016.
- [26] N. Guijarro, M.S. Prevot, X. Yu, X.A. Jeanbourquin, P. Borno, W. Bouree, M. Johnson, F. Le Formal, K.A. Sivula, Bottom-up approach toward all-solution-processed high-efficiency Cu(In,Ga)S₂ photocathodes for solar water splitting, *Adv. Energy Mater.* 6 (2016) 1501949, <https://doi.org/10.1002/aenm.201501949>.
- [27] X.B. Fan, S. Yu, F. Zhan, Z.J. Li, Y.J. Gao, X. B Li, L.P. Zhang, Y. Tao, C.H. Tung, L. Z. Wu, Nonstoichiometric Cu_xIn_yS quantum dots for efficient photocatalytic hydrogen evolution, *ChemSusChem* 10 (2017) 4833–4838, <https://doi.org/10.1002/cssc.201701950>.
- [28] N.N. Syrbu, I.M. Tiginyanu, L.L. Nemerenco, V.V. Ursaki, V.E. Tezlevan, V. Zalamai, Exciton spectra, valence band splitting, and energy band structure of CuGa_xIn_{1-x}S₂ and CuGa_xIn_{1-x}Se₂ crystals, *J. Phys. Chem. Solid.* 66 (2005) 1974–1977, <https://doi.org/10.1016/j.jpcs.2005.09.029>.
- [29] N.N. Syrbu, A.V. Dorogan, V.V. Ursaki, A. Masnik, Wavelength modulated optical reflectivity spectra of CuAl_{1-x}Ga_xSe₂ crystals, *J. Opt.* 12 (2010), 075703, <https://doi.org/10.1088/2040-8978/12/7/075703>.
- [30] M.I. Alonso, M. Garriga, C.A. Durante Rincón, M. León, Optical properties of chalcopyrite CuAl_xIn_{1-x}Se₂ alloys, *J. Appl. Phys.* 88 (2000) 5796–5801, <https://doi.org/10.1063/1.1319169>.
- [31] M.I. Alonso, K. Wakita, J. Pascual, M. Garriga, N. Yamamoto, Optical functions and electronic structure of CuInSe₂, CuGaSe₂, CuInS₂, CuGaS₂, *Phys. Rev. B* 63 (2001), 075203, <https://doi.org/10.1103/PhysRevB.63.075203>.
- [32] M.I. Alonso, J. Pascual, M. Garriga, Y. Kikuno, N. Yamamoto, K. Wakita, Optical properties of CuAlSe₂, *J. Appl. Phys.* 88 (2000) 1923–1928, <https://doi.org/10.1063/1.1305858>.
- [33] S. Levchenko, N.N. Syrbu, V.E. Tezlevan, E. Arushanov, S. Doka-Yamigno, Th. Schedel-Niedrig, M. Ch. Lux-Steine, Optical spectra and energy band structure of single crystalline CuGaS₂ and CuInS₂, *J. Phys. Condens. Matter* 19 (2007) 456222, <https://doi.org/10.1088/0953-8984/19/45/456222>.
- [34] S. Levchenko, N.N. Syrbu, V.E. Tezlevan, E. Arushanov, J.M. Merino, M. Leon, Exciton spectra and energy band structure of CuGaSe₂ single crystal, *J. Phys. D Appl. Phys.* 41 (2008), 055403, <https://doi.org/10.1088/0022-3727/41/5/055403>.
- [35] I.G. Stamov, N.N. Syrbu, B.V. Korzun, V.V. Ursaki, A.V. Dorogan, A. Masnik, Calculation of optical functions of excitons and electron transitions by means of Kramers-Kronig relations in CuAlS₂ crystals, *Mold. J. Phys. Sci.* 12 (2013) 9–17.
- [36] N.N. Syrbu, A.V. Dorogan, A. Masnik, V.V. Ursaki, Exciton spectra and energy band structure of CuAlSe₂ single crystals, *Mold. J. Phys. Sci.* 10 (2011) 143–154.
- [37] J.E. Jaffe, Alex zunger, electronic structure of the ternary chalcopyrite semiconductors CuAlS₂, CuGaS₂, CuInS₂, CuAlSe₂, CuGaSe₂, and CuInSe₂, *Phys. Rev. B* 28 (1983) 5822–5847, <https://doi.org/10.1103/PhysRevB.28.5822>.
- [38] R. Ahuja, S. Auluck, O. Eriksson, J.M. Wills, B. Johansson, Calculated optical properties of a solar energy material: CuGaS₂, *Sol. Energy Mater. Sol. Cell.* 53 (1998) 357–366, [https://doi.org/10.1016/S0927-0248\(98\)00034-8](https://doi.org/10.1016/S0927-0248(98)00034-8).
- [39] A. Soni, V. Gupta, C.M. Arora, A. Dashora, B.L. Ahuja, Electronic structure and optical properties of CuGaS₂ and CuInS₂ solar cell materials, *Sol. Energy* 84 (2010) 1481–1489, <https://doi.org/10.1016/j.solener.2010.05.010>.
- [40] A. Soni, A. Dashora, V. Gupta, C.M. Arora, M. Rerat, B.L. Ahuja, R. Pandey, Electronic and optical modeling of solar cell compounds CuGaSe₂ and CuInSe₂, *J. Electron. Mater.* 40 (2011) 2197–2208, <https://doi.org/10.1007/s11664-011-1739-1>.